Analysis of Well Test NLW-GT-01

9 March 2018

Report G1340_3

Analysis of Welltest NLW-GT-01

G 1340_9 March 2018

Author
Pieter Lingen (plingen@worldonline.nl)

Reviewed by
Bram Sieders
Christiaan van der Harst – Chief RE

Prepared for
Trias Westland
Nieuweweg 1
2685 ZG Poeldijk
The Netherlands

Prepared by
PanTerra Geoconsultants B.V.
Weversbaan 1-3
2352 BZ Leiderdorp
The Netherlands
T +31 (0)71 581 35 05
F +31 (0)71 301 08 02
info@panterra.nl

Summary

- During the 30 hours test (with 9 hours of water production) of well Naaldwijk GT-01, starting 28 Feb. 2018, the water production rates varied between 215 and 428 m^3/hr with a cumulative production of 3350 m^3.

- Evaluation of the test indicates an average reservoir permeability of about 700 mD if all layers of the 83 m thick reservoirs contribute.
  - The observed permeability is the radial permeability. The average permeability between NLW-GT-01 and its doublet well might be higher because of placement parallel to the dominant fault structure. An interference test is therefore recommended during the test of the doublet well (NLW-GT-02).

- Total skin is 1.4 at 427 m^3/hr, but -0.2 at low rate. This indicates that there is no formation damage.

- The well test interpretation indicates the presence two flow barriers at distances of around 250 and 700 m. These barrier are probably faults, but do not have to be fully sealing. The build-up is too short to determine if these two barriers are parallel or at an angle. Also, their distance depends on the unknown contributing sand thickness and the estimated compressibility. The only mapped seismic fault is situated 700m from the well (see Figure 1).

- Static reservoir pressure at 2317 mtv is 234 bara.
- Reservoir temperature is about 87 °C.
- Transient flow capacity (PI) after 30 hours flow is about 24 m^3/hr/bar.
- The correction for the changing temperature of the water column between the ESP and BHP is similar as found in other Delft reservoir water wells. The continuing increase in pressure difference between the ESP and bottom gauges with the cooling of the water column indicates a water salinity of 120 kg/m^3 NaCl equivalent.

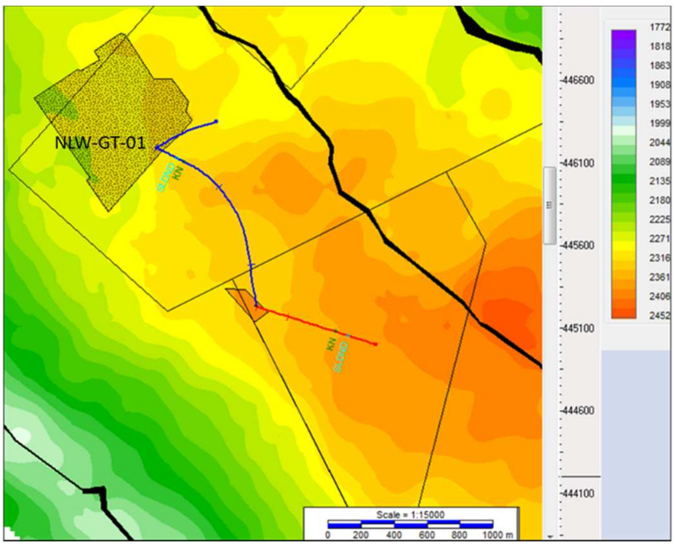

Figure 1 - Top Structure Map Delft sandstone (by T&A); Well NLW-GT-01 is shown in blue, planned well NLW-GT-02 is shown in red. Faults are represented by thick black lines.

Resultaten van de put test

Gegevens voor test interpretatie	Waarde	Dimensie
Naam van de put	NLW-GT-01	
Top aquifer	2604	m (langs boorgat)
“	2312	en m (TVD)
Basis aquifer	2752	m (langs boorgat)
“	2440	en m (TVD)
Netto dikte Aquifer	83.4	m (TVD)
Netto/bruto aquifer	89	%
Gemiddelde porositeit aquifer	18.7	%
Zoutgehalte formatiewater van sample	120	kg/m3
Verwachte max. temperatuur geproduceerde water[1]	87	ºC
Casing 20“	1158	m tv
Casing 13 3/8”	2168	m tv
Casing 9 5/8”	3773	m tv
Diameter boorgat bij aquifer	9 5/8	Inch
Top productie-interval/filter (6 5/8 x 7”)	2604	m (langs boorgat)
“	2312	m (TVD)
Basis productie-interval/filter (6 5/8 x 7”)	2752	m (langs boorgat)
“	2440.4	m (TVD)
Weerstand over screens[2]	0	bar
Locatie pomp	752	m (ah)
Locatie meetsonde voor druk	752	m (tv)
Locatie diepe wireline gauge	2600	m (langs boorgat)
“	2317	m tv
Meetreeksen Puttest[4]	Eind ESP druk, bar	Eind Debiet, m3/uur
Flow 1	64.4	215
Flow 2	61.1	327
Flow 3	57.1	428
Flow 4	64.7	226
Flow 5	56.4	427
BU	70.65	0
Uitkomsten test interpretatie en analyses		
Skin	-0.25 to 1.43	
H	83.5	m
K	700	mD
KH	58.1	D*m
PI (transient 30 hrs)	24.1	m^3/hr/bar
Two flow-barriers/baffles at approximately	270 and 670	m from well
Deviatie		

Diepte langs boorgat	Diepte m tv	East	North
0	0	76147,00	445237,00
2604	2312		
Mid reservoir ~2670	2376		
2752	2440		

1 Deze temperatuur wordt als gemiddelde aquifer temperatuur beschouwd
2 Geen meting van weerstand over filter

Contents

1 Introduction

The geothermal well NLW-GT-01 (Naaldwijk) was production tested for some 30 hours.
The test started 28/02/2018 08:05 with a multi-rate test for 9.5 hours, followed by a shut-in period of 21 hours.

The ESP generated production rates were increased in steps from 215 to 428 m^3/hr, with a final flow period of 3.5 hours at 427 m^3/hr. Cumulative water produced was about 3350 m^3. The pressure and temperature data were recorded both by the ESP gauge at 752 mtv and two high-accuracy gauges on wireline at 2317 mtv.

The well was produced from Delft and Alblasserdam sandstones, 2312 – 2427 mtv, covered by sand exclusion screens. The total net sand thickness is estimated at 83.4 m.

The correction formula, as determined from the ESP data in combination with the downhole gauge data, was used to determine the water salinity and as basis for an analysis based only on ESP data for the target reservoir. During the build-up, 4 instances of wireline shrinkage have been observed, but the resulting pressure steps were too small to have a significant effect on the analysis.

2 Reservoir and Rate data

The average porosity of the two layers has been estimated at 18.7%. Net thickness is 84.3 mtv.

The wellbore radius Rw has been set to the drilling bit size of 10”, or 0. 417 ft. In view of the deviation of the well with an average angle of about 30 degrees through the reservoir, the wellbore radius was adjusted to $Rw*\sqrt{\{(1+1/\cos\alpha^2)/2\}}$ = 0.45 ft, for the analysis with a vertical well model.

The reservoir temperature is estimated at 87 °C as the extrapolated maximum observed BHP gauge temperature at the highest rate.

The water viscosity and water compressibility have been based on the salinity: μw = 0.433 cP and Cw = 2.5E-6 psi^{-1} respectively. A value of Cf = 3.5E-06 psi^{-1} was used for the pore compressibility.
The porosity and total compressibility (Cw + Cf) may have to be adjusted once the interference test with the next well is completed.

Table-1 lists the used rate sequence during the production test, as obtained from the rate data presented in Fig 1, chapter 3.

Table-1

Hours since start	Flow rate m^3/hr	Flow Rate, b/d
1.02	215	32450
1.0	327	49360
2	428	64600
2	226	34120
3.5	427	64460

3 Recorded Pressures, BHP and ESP.

Fig-2 shows the original downhole gauges, together with the flowrates and temperatures. As both gauges show practically the same curves, only the bottom gauge, G2, has been used for analysis.
As these gauges are just at top reservoir, the cooling during the build-up is only relatively small (from 86 to 84 °C). The cooling effect at the ESP is more significant as shown in Fig-3 (declining from 86 to 65 °C).

The practice to record all data per second is leading to a very large data volume. As the early build-up is always disturbed by wellbore effects, 3 or 4 points per minute are sufficient for the analysis, reducing the time of data preparation. In the presented plots the data have been filtered and not more than 500 data points have been used to describe the whole test. These points still use all data by applying a moving-average filtering on the original data set.

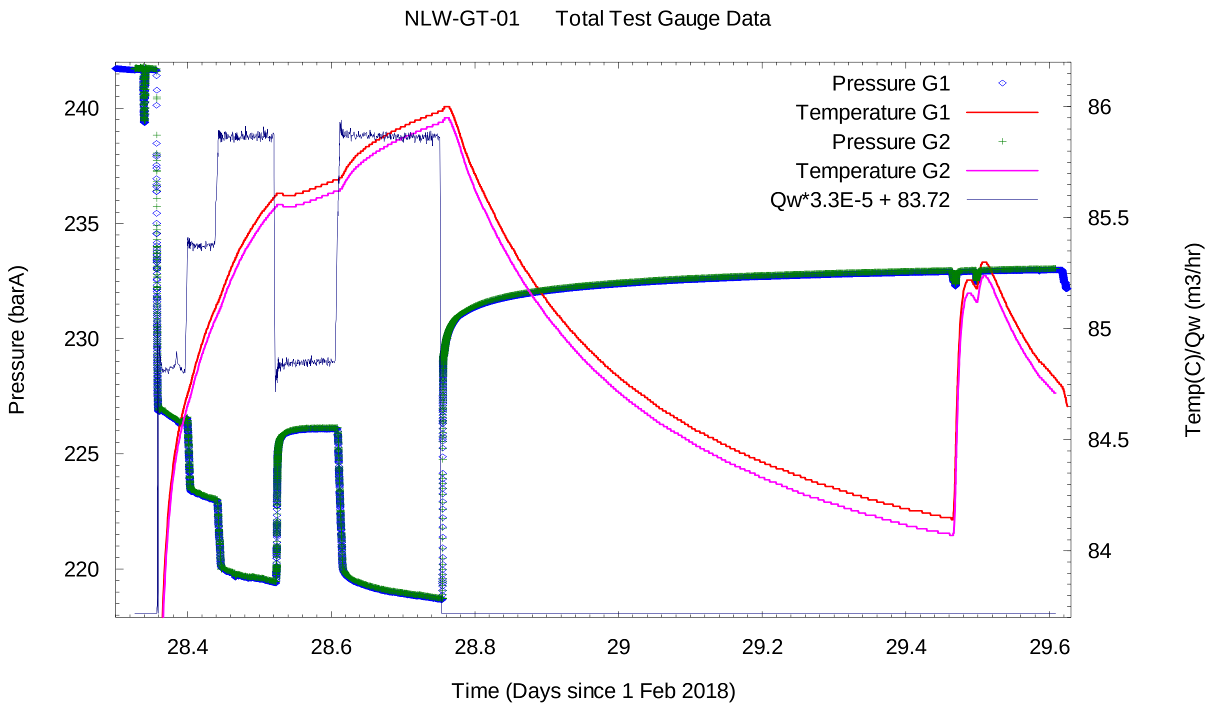

Figure 2 - Pressures recorded by Bottom Hole pressure gauges, flowrates and temperatures.

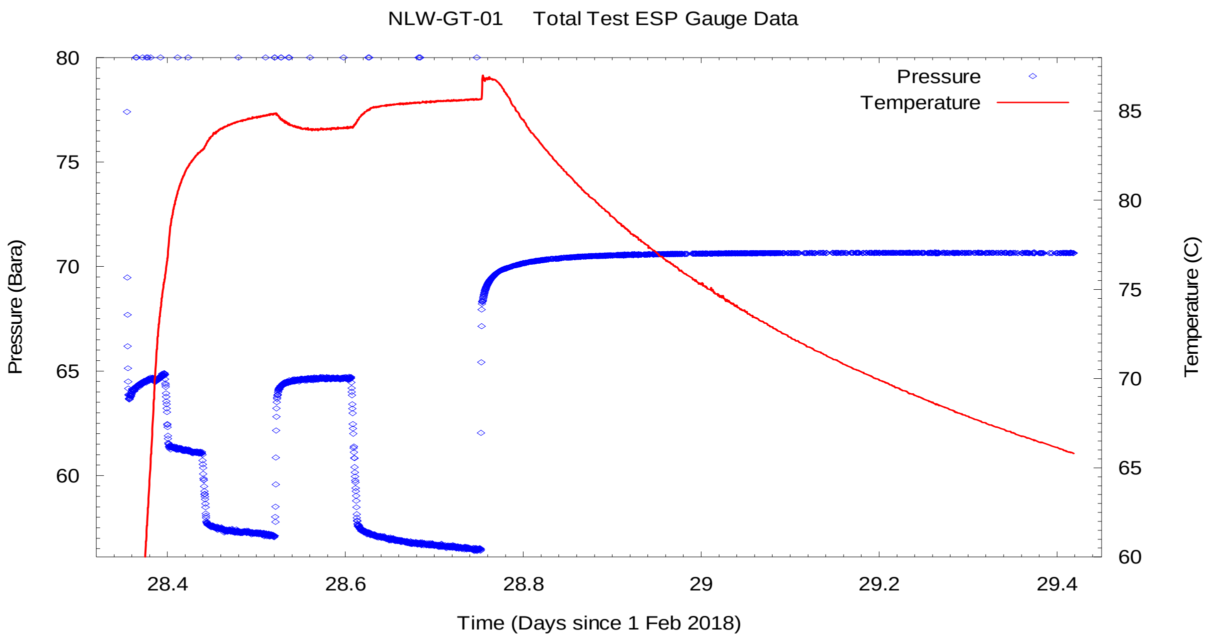

Figure 3 - Pressures and Temperatures recorded by pressure gauges at the ESP depth.

4 Corrections during build-up

The pressures of the downhole gauge were correlated with those of the ESP, 1565m higher, as function of the ESP temperature in Fig-4. The resulting correction formula, only matching ESP temperatures below 78.5 °C, is:

DP = CDC*L*{1050.2+0.4054*(86-T)-0.00238*(86-T)**2}

With DP the pressure correction, CDC a constant [CDC= 9.8063E-5 if pressure in bar] and L (= 1565) the distance in meters between ESP and bottom gauges, and T the current ESP gauge temperature in °C. With a maximum recorded BHP temperature of 86, this maximum temperature was used in the equation shown above. This formula can thus be used to calculate BHP pressures from pressure data at ESP depth.

The blue points are the pressure differences between BHP and top gauge, with the fitted function through those points in red (hardly visible as the red line is covered by the blue points). The green points are the blue points minus the red fitted curve, plotted at the large right-hand scale. The inaccuracy is relatively small and caused by the limited resolution of the ESP gauge.
Four very small steps can be seen in the green data points, caused by the shrinkage of the wireline. As these steps are very small, no correction to the build-up data has been applied.

The function, displayed in Fig-4 and used to calculate the pressure difference between ESP depth and Bottom Hole depth, is very similar to that obtained from the test data of other Delft reservoir wells.

The water salinity was calculated from the pressure difference of 161 bar at an average column temperature of 85.7 °C. With a vertical distance of 1565m this gives a pressure gradient of 0.1029 bar/m, or 1049 kg/m3 which indicates a salinity of 120 kg/m3 NaCl equivalent {equivalent means that all the different salts (all metals can form salts) are translated to the amount of NaCl that gives the observed water density}, using the curves presented in Appendix 1.

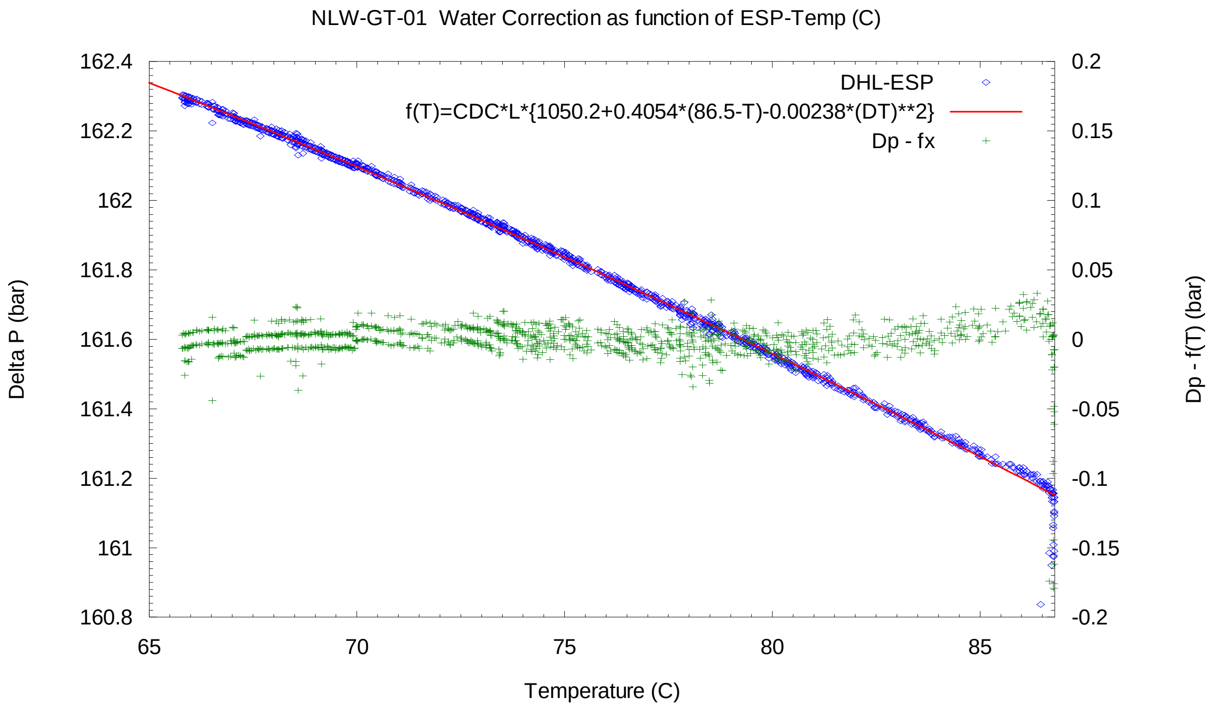

Figure 4 - Pressure correction to convert pressures at ESP depth to BHP as a function of Temperature.

5 Analysis method

The pressure test analysis is carried out by the match of the most appropriate analytical well/reservoir model response with the total test history. In this way, no approximations have to be used, as for the model response the flow equations are solved for the reported flow rates. It should be noted that each pressure point measured in a well depends on the total previous rate history of that well, both in the real reservoir as in the analytical model. Analysis of only one rate period, ignoring the rate history, can thus give only an approximation of the actual reservoir/well parameters.

The standard analysis results in a split of the observed productivity at reservoir depth (otherwise Tubing Head Pressure data would be sufficient) into the reservoir potential (k*h/µ) and an extra flow resistance, the skin, S. This skin is any deviation of the effective wellbore radius, rw, and represents formation damage of the reservoir, which may be caused by drilling (mud invasion), resistance over the sand exclusion screens, by deposits of evaporates, etc. Some forms of skin can be removed (e.g. by a well clean-out with coiled tubing, injection of acid or by temporary production at a high production rate). The skin includes also the flow resistance over the vertical conduit between reservoir and pressure gauge; this type of skin is rate dependent and can therefore be determined by testing with at least 3 different flow rates, so that the (rate independent) damage skin can be calculated.
The skin can also be negative as a result of acid stimulation (increased permeability just around the wellbore), fraccing or sand production (enlarging the effective wellbore radius), or by the perforation tunnels (in this well).

From a detailed analysis of mainly the build-up pressure data, information about the presence and distance of flow barriers in the reservoir (faults, channel boundaries or sedimentological changes) can be obtained.

As no deviated well model is available, a vertical well model has been used, based on the assumption that the flow in the reservoir at some distance from the well will be horizontal and thus the same for a deviated and a vertical well. This is usually a valid assumption, as the vertical permeability is normally lower than the horizontal permeability in sandstone. The reservoir geometry shown by the top structure map in Fig. 1 shows that there are parallel faults. The model-well can be placed in a rectangular bounded reservoir as indicated in the sketch below. Models with 1 boundary (other boundaries placed outside the radius of investigation), a channel geometry, 2 reservoir layers and 2 boundaries were tried. A schematic overview of these models is shown in Fig 8. These models are always simplifications of the actual reservoir geometry and can only take very basic changes in sedimentology into account. The model also assumes a constant reservoir thickness. A perfect match is therefore not always achieved. Comparison of the different models is discussed in Chapters 6 and 7.

The matched-model response for early times usually deviates from the observed pressures. These early build-up pressures are expected to be influenced by water hammer, the latent motor heat of the ESP motor and possibly by cold-water fall-back. These temporary effects are hard to model in detail and have no impact on the estimation of reservoir properties.

The model response to the test rate history - including all flow and shut-in periods (even the pre-test flow periods for which no pressure data are available) - is obtained by the principle of super-position. The parameters of the model are varied until the difference between model response and observed well response is minimal.

The transient Productivity Index (PI) is obtained from the last point of the underlying single-rate model response, and is the best estimate of the longer-term PI.

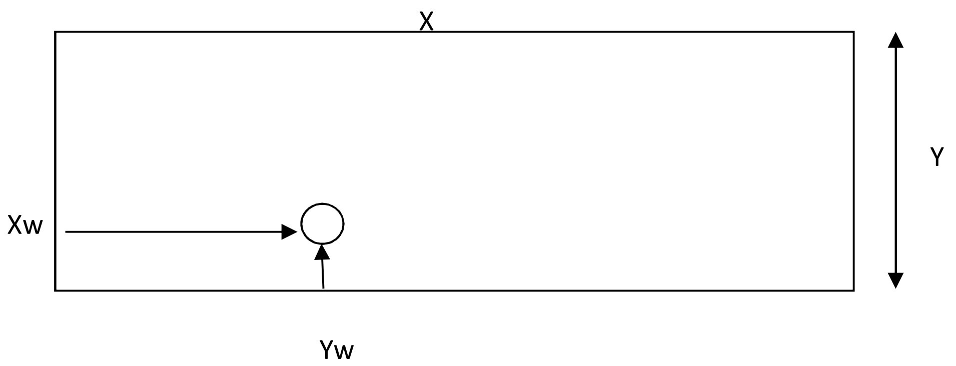

Figure 5. Sketch of a rectangular reservoir, where the well is situated at distances Xw and Yw from the barriers.

6 Analysis of corrected pressure data

The downhole gauge pressures have been matched with above described models. Fig-6 shows an example of the match of the final build-up, both for pressure and for the derivative of the pressure. The pressure derivative displays more information than the pressure and is therefore used to draw conclusions about the reservoir geometry and the presence of flow barriers.
NB: The (Agarwal) effective time is used in order to obtain a straight-line Horner plot for this test with a short and varying rate history and a relatively long build-up. The total build-up time in this figure is 17 hrs, with a final effective time of only 4.87.

The double wellbore storage behaviour as displayed on the left hand side in Fig-6 is seen in all hot-water wells and is thought to be caused by the “water-hammer” effect: The kinetic energy of the flowing water is abruptly changed into the potential energy of the water level in the annulus, rising above the static water level, compressing the gas present in the top of the annulus. By applying an increasing wellbore storage in the model, this water-hammer effect can be approximated. But in order to get the best match with the more relevant late build-up data (on the right hand side of Fig-7), a non-optimal match of this early wellbore storage has been accepted. The late build-up points were given a higher weight-factor.

Following the moderately accurate match of the initial build-up, caused by these wellbore effects the match of the data after 0.1 hour is good. The late build-up, after 1 hour effective time, is influenced by the presence of one flow barrier at approximately 320 m from the well. The model with only one flow barrier does not match the late build-up pressures of Fig-7 very well, indicating that possibly a second flow-barrier (faults) or baffle to flow (sedimentological change) is present within the radius of investigation of this well test.

Note that the build-up of Fig-8 is longer than that of Figs-6 and -7. This is caused by two short periods with some flow, caused by removal of the ESP. The bottom gauges kept on registering the pressure in the closed-in well. These additional pressures can only be matched by the introduction of a second flow-barrier.

Fig-7 presents the comparison of 3 reservoir geometry models: Model-1 has one barrier at 330 m; Model-2 is rectangular and has two barriers, one in the X-direction at 670 m and one in the Y-direction at 270 m; Model-3 is for a well in a flow channel with two parallel boundaries, with a width of 710 m and the nearest channel boundary/baffle at 240 m. The 4 steps in the late derivative are caused by the upward movements of the gauges, caused by the shrinking wireline; this usually happens in 'jerks' as moving friction is less than static friction. Considering these steps, the two-barrier models seem to provide a better match. Although it should be clear, that these barriers are not necessarily fully sealing.

Both two-barrier models give a similar match of the derivative and the build-up extension and no clear preference can be established.

The selection of the preferred model should also be based on seismic and sedimentological information, the top structure map is shown in Fig 1. All models however have one aspect in common: a barrier at around 270-320 m. This barrier is not seen on the map and may be a minor fault (not visible on seismic), a channel boundary or a sedimentological change. Further away from the well at a distance of 700 m there may be a second barrier, but the test was too short to draw any firm conclusions on this second feature. On the top structure map the faults run in a NW-SE direction and the nearest fault to the well (visible on seismic) is about 700m away. So the 'preferred model' is a mix of the 5 models presented in this note and incorporates 2 layers, a barrier at 300m and possibly a second feature around 700m from the well.

The resulting model parameters demonstrated a reasonable fit with a permeability of 700 mD for the main Delft sandstone, a static reservoir pressure of 234 bar (at 2317 mtv) and a relatively low skin of 1.4 at the final, high, flow rate. The Productivity Index after 30 hrs is about 24 m3/hr/bar.

The skin value has been determined at all flow periods, by matching the same model on all final flowing pressures:

Flow rate:	215	327	428	226	427
Skin :	2.35	1.96	1.64	0.64	1.43

This indicates that the well was still cleaning-up during the first two flow periods of 1 hour with a declining skin at increasing rate, but nearly stabilised during the low rate at 226 m3/hr.
NB: the slight downwards curvature of the flowing pressures at this final high flowrate shows some further formation damage reduction (reducing skin from 1.64 to 1.43). The flowrate dependency of the skin is

caused by the friction over the flow conduit and perforations. Extrapolation of the two final skin values (0.64 and 1.43) to zero rate result in the real damage skin of -0.25, which is probably caused by the length of the perforation holes into the reservoir and highlights the absence of formation damage.

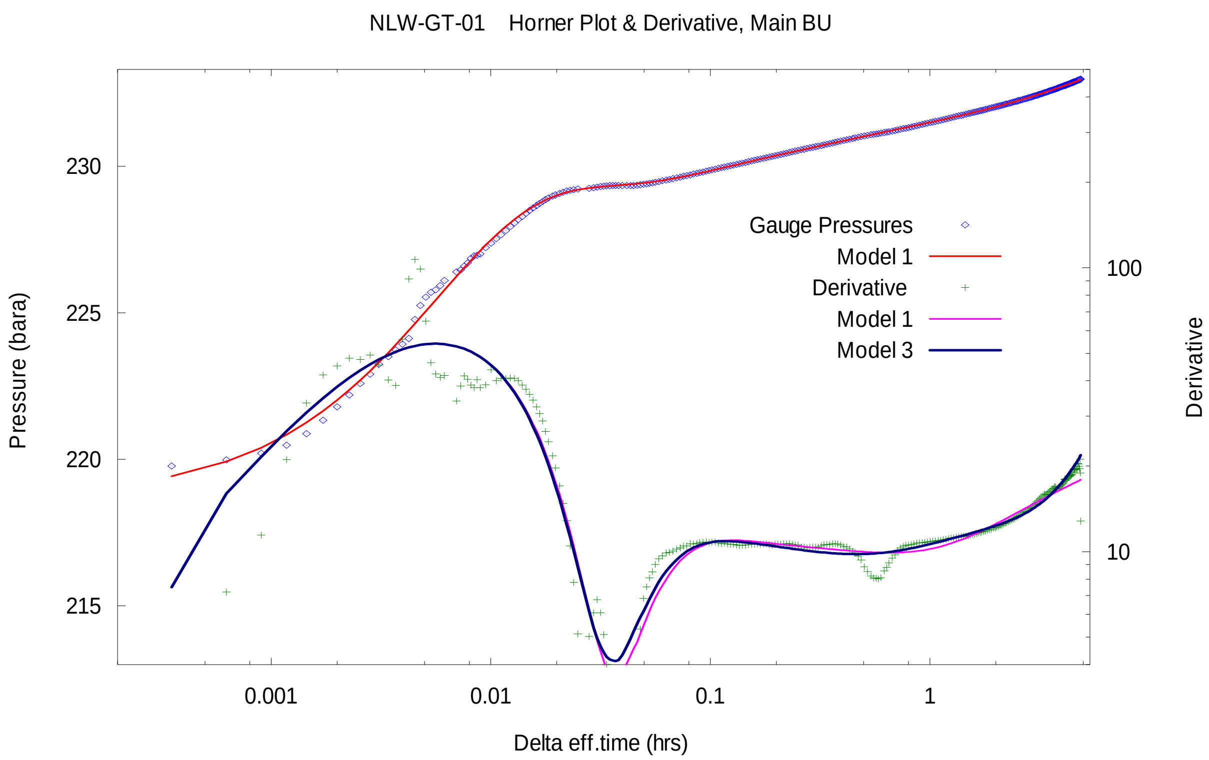

Figure 6- Comparison of measured and modelled Pressure response for Pressure (in bar) and Derivative, showing a good match between the model and the measured data.

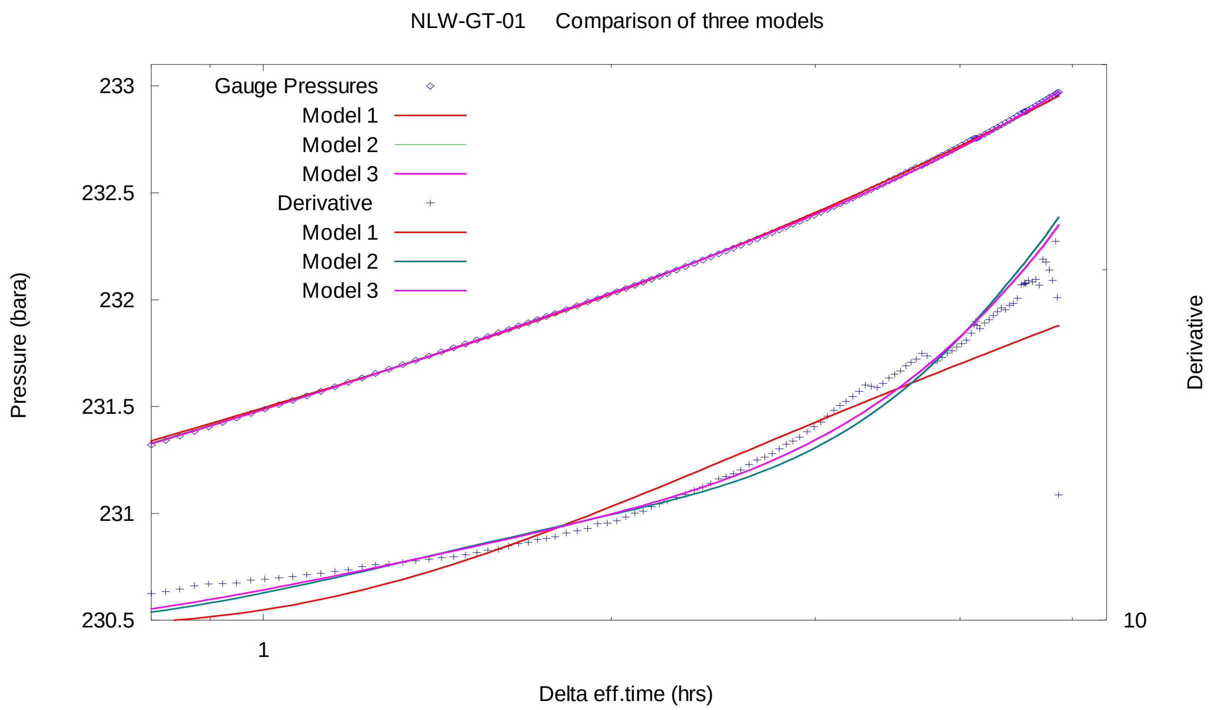

Figure 7 - Comparing the pressure (in bar) response of 3 models with different reservoir boundaries.

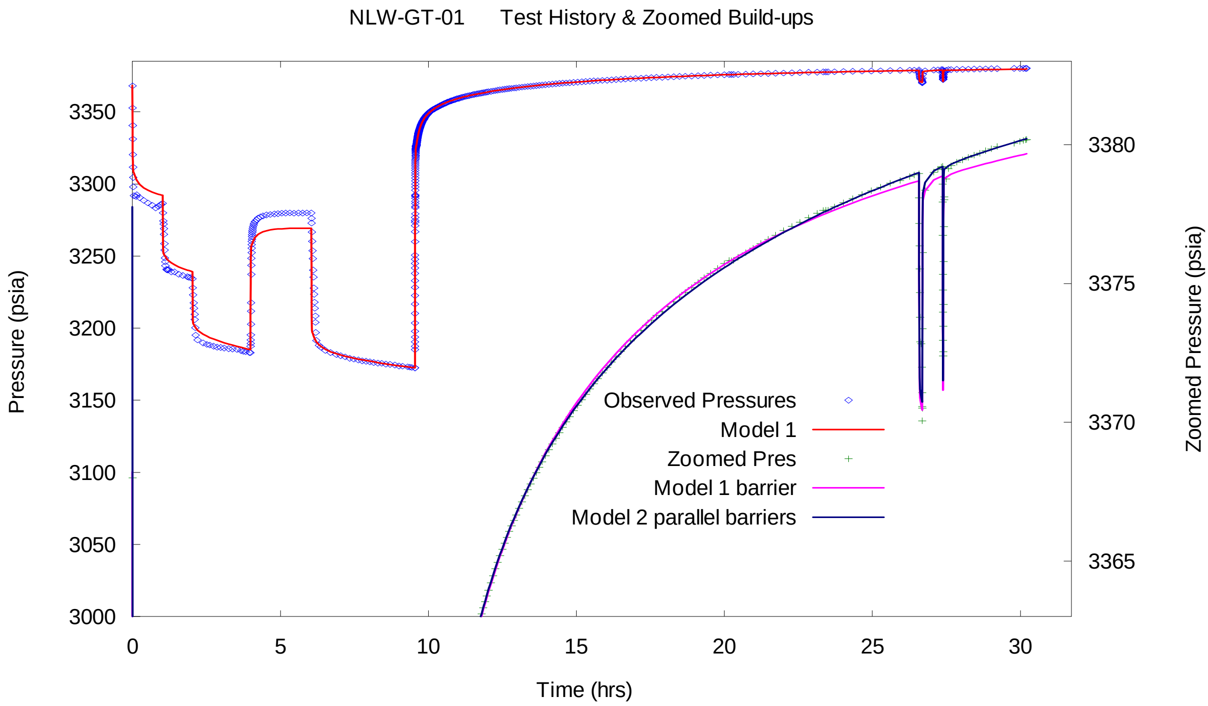

Figure 8 - Comparing the pressure (in bar) response of 2 models on whole test history.

8 Alternative models

A 4th Model was tried by M. Talebian of Panterra which had 1 barrier and 2 reservoir layers and finally a 5th model was investigating the impact of a baffle in a radial configuration. Fig-9 shows three different reservoir models. The pressure responses of these models were comparable to the 2-boundary model discussed in Chapter 7 and demonstrate that the test was too short to draw any firm conclusions about the presence of a second boundary/baffle. The slight increase of the derivative on the right-hand side of the graph is probably caused by a change in sedimentology 500-700 m from the well.

Fig-10 shows a comparison of the build-up pressures in a Horner plot for models with a single reservoir layer and 1 & 2 boundaries and a model with 2 reservoir layers and 1 boundary. The match with the 2 layer model seems to be slightly better at later times of the pressure build up, although the response of all models is comparable.

Fig-11 shows a comparison of the Pressure derivative of the type curves for models with 1 layer and 1 & 2 boundaries and a model with 2 layers and 1 boundary. The main difference occurs later in the test where the data scatter is relatively large. None of the models is able to reproduce the derivative data points exactly, however the 2 layer model with 1 boundary seems to provide a reasonable fit. The differences between the models are relatively small and the all deliver similar reservoir permeabilities and skin factors.

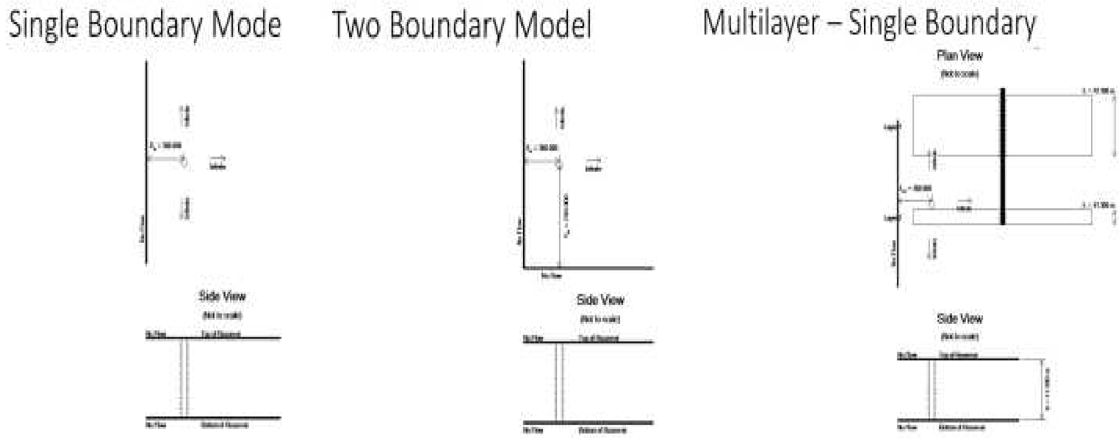

Figure 9 - Different types of well models used to match the measured pressure data.

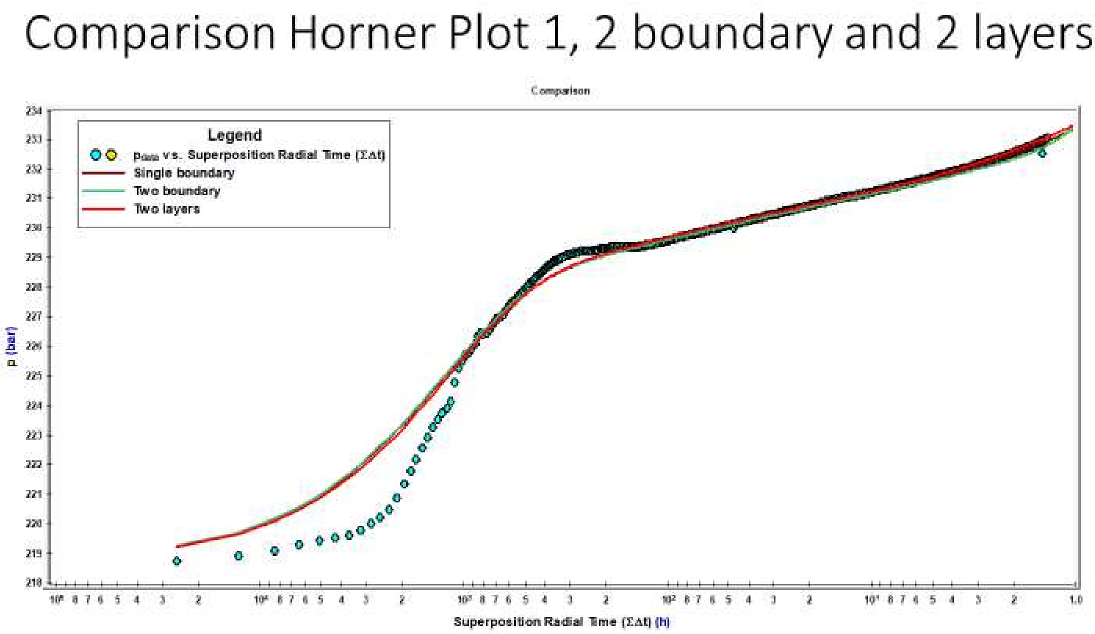

Figure 10 – Comparison of the pressure build up in a Horner plot for the models with 1 & 2 boundaries and the model with 2 layers and 1 boundary.

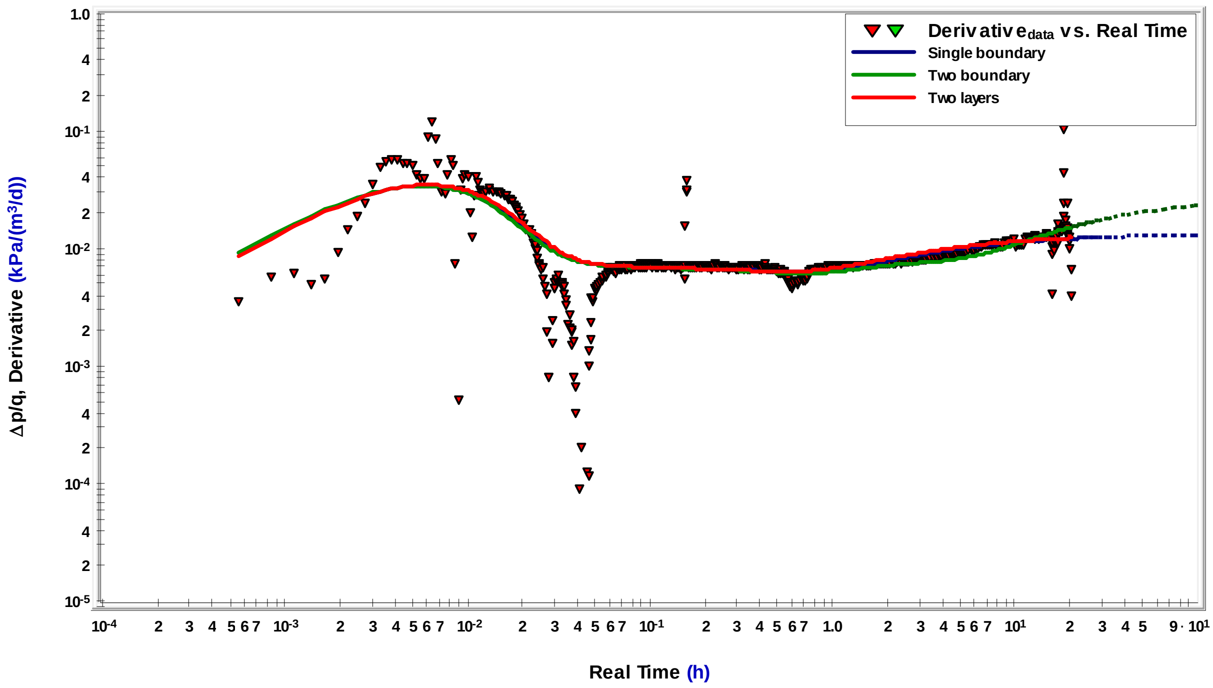

Figure 11 – Comparison of the pressure derivative from the Type curves for the model with 1 and 2 boundaries and the model with 2 layers and 1 boundary.

9 Conclusions and Recommendations

The Naaldwijk well test has been successful in establishing an accurate estimate of reservoir permeability of about 700 mD, and demonstrates that there is a very low skin factor (close to 0) and no formation damage. The real permeability may be higher if the contributing sand thickness is lower.

The observed total net sand thickness of 83 m is slightly thicker than the pre-drill estimate of 77m. The reservoir pressure (234 bar) and temperature (87 °C) are in line with expectations.

The (transient 30 hrs) PI of the well is high at 24 m3/hr/bar and suggests that a successful geothermal project can be envisaged using the NLW-GT-01 well and the planned second well of the doublet.

There appear to be two flow barriers near the well. The nearest is most certain at a distance of 250 to 320 m from the well. The length of the actual build-up was too short to accurately estimate the distance and position of a second flow barrier. A longer build-up time of at least 24 hours is therefore advised for the well test in the second well of the doublet, once completed.

It is advised to conduct an interference test with the doublet well in order to determine whether there is a barrier that could cause resistance to flow between the 2 wells. Based on the current top structure map and fault interpretation (see Fig 1) it is expected that the main faults run in NW – SE direction, and the nearest fault is mapped about 700 m away from the well. This fault could be seen as the second flow barrier. Due to the relatively large reservoir thickness in the targeted area, the likelihood of encountering a sealing fault perpendicular to the existing fault grid between the 2 wells is considered to be very small. A better definition of the boundaries around this doublet and the long-term steady-state PI can also be obtained from the interference test results.

10 Appendix.

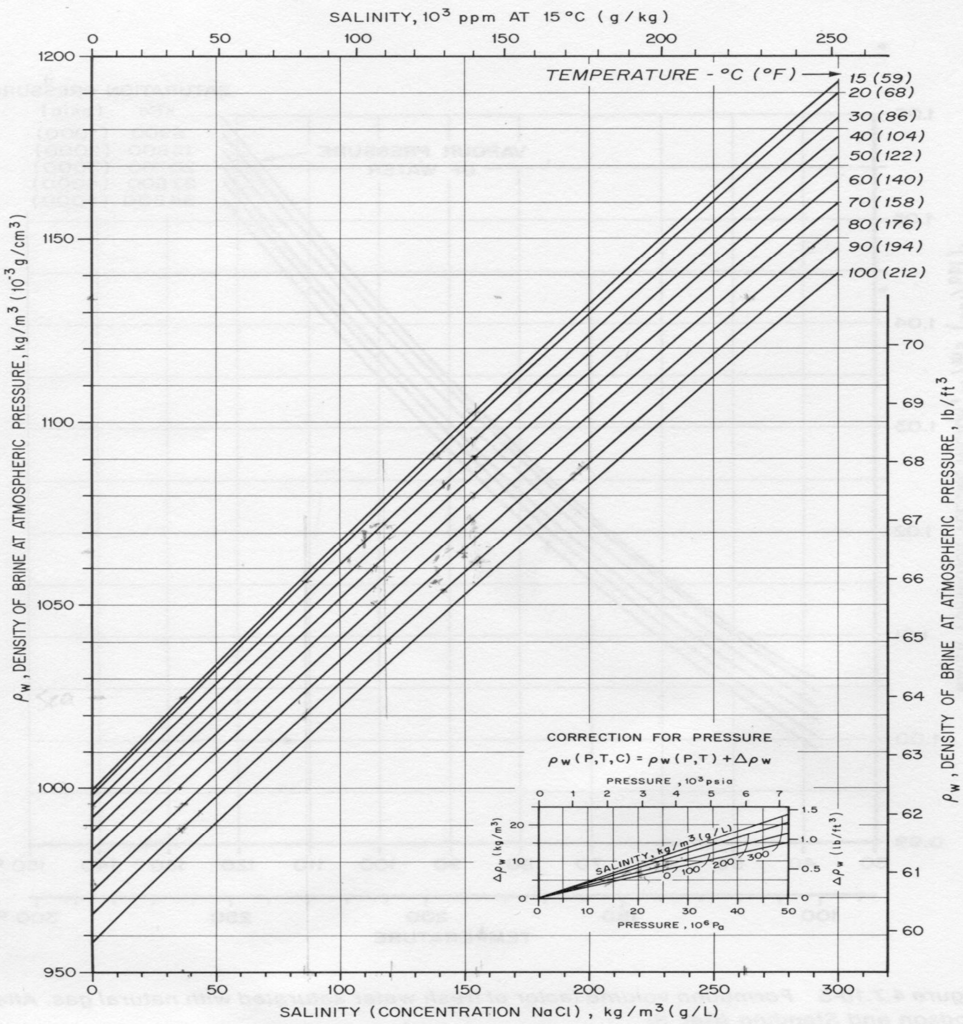

Figure 4.7.10-6 Water density as function of dissolved solids. After Long and Chierici (Ref. 35)

Appendix 1. Water density as function of Salinity